Journal of Materials Chemistry C

ROYAL SOCIETY OF CHEMISTRY

PAPER

View Article Online
View Journal | View Issue

Cite this: J. Mater. Chem. C, 2020, 8, 1089

Responsivity improvement of a packaged ZnMgO solar blind ultraviolet photodetector *via* a sealing treatment of silica gel†

Xing Chen,[ab] Liyan Wang,[ab] Kewei Liu,*[ab] Zhenzhong Zhang,[ab] Binghui Li,[ab] Jiabin Wu,[ac] Jingyuan Wang,[ac] Yingxue Ni[ac] and Dezhen Shen*[ab]

Received 3rd October 2019,
Accepted 28th November 2019

DOI: 10.1039/c9tc05427h

rsc.li/materials-c

Packaging is one of the most important procedures of the fabrication of photoelectric devices, such as ZnMgO solar blind ultraviolet (UV) photodetectors. The roles of packaging are: electrically interconnecting an unpackaged photodetector and pin as well as fixing it, and protecting the unpackaged photodetector from external dirt, humidity and atmosphere. Nowadays, the research on the ZnMgO solar-blind UV photodetectors has well developed. However, the research on the packaging of these photodetectors are rare. In this study, we have focused on the packaging of ZnMgO solar blind UV photodetectors. After a direct wire bonding method between steel wires and unpackaged photodetectors by conductive silver adhesives and a sealing treatment by silica gel, the ZnMgO photodetector was packaged, and the responsivity of the device was found to increase after the packaging. A −3 dB cutoff wavelength of 295 nm and a responsivity of 191 A W^{-1} were achieved under a bias of 10 V. The 90–10% decay time of the device was 280 ms, and the dark current of the device was 115 pA under a bias of 10 V. Moreover, the stability of the ZnMgO-based solar blind photodetector obviously improved due to the well-sealed packaged structure.

Introduction

The ultraviolet (UV) radiation below 280–300 nm can be strongly absorbed by the stratospheric ozone; thus, the UV radiation from the sun in this range cannot penetrate the atmosphere to reach the earth's surface, and this is called the solar blind region. The photodetectors that work only in the solar blind region can detect a very weak signal under sun due to the absence of sky background interference. Therefore, the solar blind photodetectors have many potential applications, such as in flame detection, missile alarming, high-pressure arc discharge detection, environmental monitoring, and nonlinear-of-sight optical communications.[1–6]

Nowadays, solar-blind UV photodetectors based on wide-bandgap semiconductors, such as AlGaN,[7,8] ZnMgO[9–13] and β-Ga_2O_3,[14–28] have attracted significant attention. Benefiting from the rapid development of their light emitting diodes (LEDs) and related process technology,[29] AlGaN-based photodetectors exhibit excellent performance than other wide-bandgap semiconductor devices. However, with an increase in the Al composition for solar blind detection, the performance of the AlGaN photodetectors rapidly becomes poor due to the obvious degradation in the crystal quality. Among the wide-bandgap semiconductors, ZnMgO has many unique properties, such as low defect density, high saturated carrier drift rate, low cost, and a wide bandgap tuning range (3.37–7.8 eV).[30–33] Therefore, ZnMgO-based materials have been regarded as some of the most promising materials for the fabrication of high performance solar-blind UV photodetectors.

According to the previous reports, the responsivity of the ZnMgO solar-blind UV photodetectors often range from 0.01 A W^{-1} to 0.3 A W^{-1}.[10,11,34–36] Although several devices with relatively high responsivity can be achieved,[12,13] a method to improve the responsivity of such devices is still needed. Moreover, it is well known that ZnMgO-based materials have potential application uses such as humidity sensor and oxygen sensor.[37,38] Alternatively, the ZnMgO-based materials are very sensitive to the humidity and oxygen, and the unpackaged ZnMgO-based photodetectors have a poor stability due to the influence of the humidity and oxygen. Packaging is one of the most important procedures for the fabrication of photoelectric devices. However, the research on the packaging of ZnMgO photodetectors is rare. In this study, to the best of our knowledge, the first research on the packaging of a ZnMgO solar blind UV photodetector is proposed. The responsivity

[a] State Key Laboratory of Luminescence and Applications, Changchun Institute of Optics, Fine Mechanics and Physics, Chinese Academy of Sciences, Changchun 130033, P. R. China. E-mail: liukw@ciomp.ac.cn, Shendz@ciomp.ac.cn
[b] Center of Materials Science and Optoelectronics Engineering, University of Chinese Academy of Sciences, Beijing 100049, P. R. China
[c] Photoelectric Detection Research Department, Changchun Institute of Optics, Fine Mechanics and Physics, Chinese Academy of Sciences, Changchun 130033, P. R. China

† Electronic supplementary information (ESI) available: Fig. S1. EDS spectra of ZnMgO films. Fig. S2. UV-Vis transmission spectra of silica gel. See DOI: 10.1039/c9tc05427h

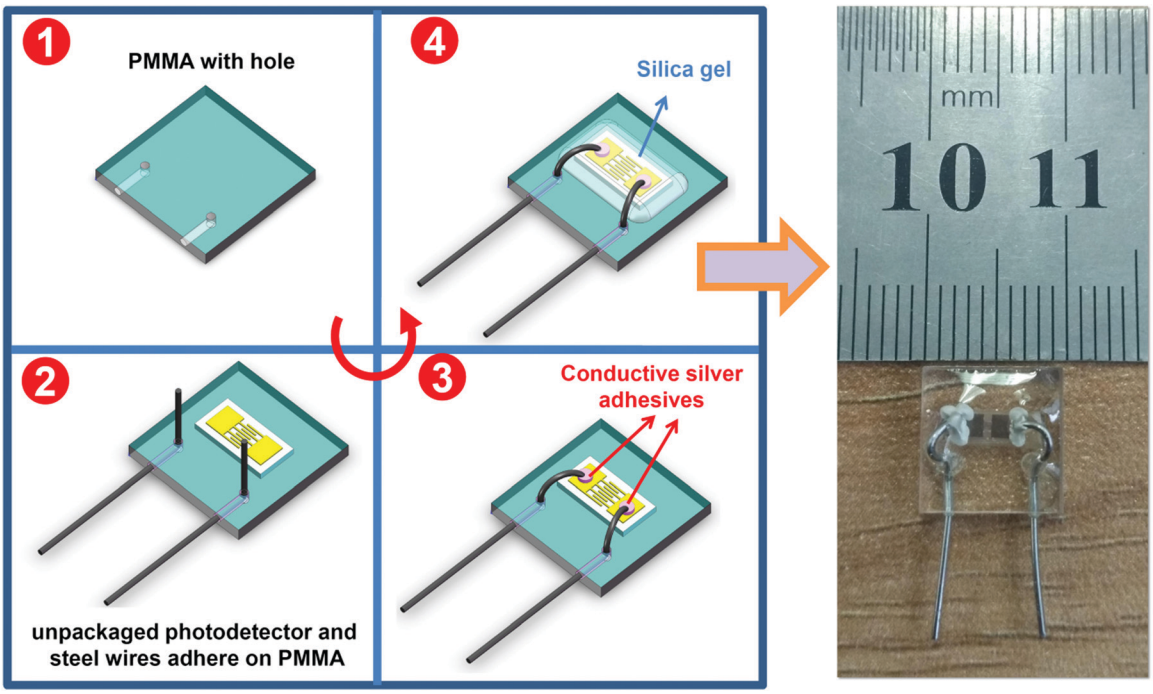

Fig. 1 Schematic of the packaging of the photodetector and the photograph of the packaged photodetector.

of the photodetector could be improved by a packaging treatment. Moreover, the 90–10% decay time could be maintained at 280 ms after the packaged photodetector is exposed to air for 6 months.

Experimental

Synthesis and characterization of ZnMgO films

ZnMgO films were fabricated on a-sapphire substrates by a molecular beam epitaxy (MBE) system, and 6 N-purity zinc and 5 N-purity magnesium held in thermal Knudsen cells and 5 N-purity O_2 activated in a radio frequency plasma source were selected as precursors. Prior to their growth, the substrates were treated with N_2 at 950 °C for 60 min to remove possibly absorbed contaminants. During the growth, the chamber pressure was maintained at 10^{-3} Pa, and the substrate temperature was kept at 350 °C. The radio frequency power was fixed at 300 W with an O_2 flow rate of 0.96 sccm.

The samples were characterized *via* scanning electron microscopy (SEM) (HITACHI S-4800), energy dispersive X-ray spectrometry (EDS) (GENESIS 2000 XMS60S), X-ray diffraction (XRD) (D8 FOCUS, BRUKER) (using Cu Kα radiation, $\lambda = 0.154$ nm) and UV-Vis transmission spectrometry (Shimadzu UV-3101PC).

Fabrication and characterization of the photodetectors

Schematic of the packaging of the photodetector and the photograph of the packaged photodetector is shown in Fig. 1. After the epitaxy of the ZnMgO films on the a-sapphire, Au interdigital electrodes (30 nm thick) were prepared on all films *via* photolithography and a wet etching procedure to form a metal–semiconductor–metal (MSM) unpackaged photodetector (named as U-PD). After the fabrication of U-PD, two sections of a steel wire with a diameter of 0.5 mm were fixed in a polymethyl methacrylate (PMMA) (10 mm × 10 mm × 3 mm) using epoxy resin. After that, the U-PD was adhered on the PMMA using epoxy resin too. Then, steel wires were pressed on the two electrode areas of the U-PD and fixed using conductive silver adhesives. Finally, the U-PD was sealed by silica gel with a thickness of 0.5 mm. Using direct wire bonding, a simple and rapid fabrication of the solar blind photodetector was achieved without comprehensive metallization processes, and the packaged photodetector was named as P-PD. A 200 W UV enhanced Xe lamp with a monochromator was used to investigate the spectral response properties of the photodetectors. The current–voltage (*I–V*) properties and the transient response spectra of the photodetectors were measured using a semiconductor device analyzer (Agilent B1500A) and a Hg lamp (254 nm).

Results and discussion

The ZnMgO film was characterized *via* SEM, XRD and UV-Vis transmission spectroscopy. It can be seen in Fig. 2(a) that the ZnMgO film has a smooth and uniform surface. Fig. 2(b) shows a typical cross-sectional SEM image, indicating that the thickness of the ZnMgO film is around 340 nm. Moreover, the result of EDS indicates that the composition of the films is $Zn_{0.61}Mg_{0.39}O$ (Fig. S1, ESI†). The XRD pattern of the sample is shown in Fig. 2(c). Besides the diffraction peak of the a-sapphire substrate, only one diffraction peak located at $2\theta = 35.14°$ can be observed, which corresponds to the (0002) orientation of wurtzite ZnMgO. In addition, the full width at half maximum (FWHM) of the (0002) peak of wurtzite ZnMgO is around 0.16°, indicating that the film has a good crystalline quality. Fig. 2(d) shows the UV-Vis

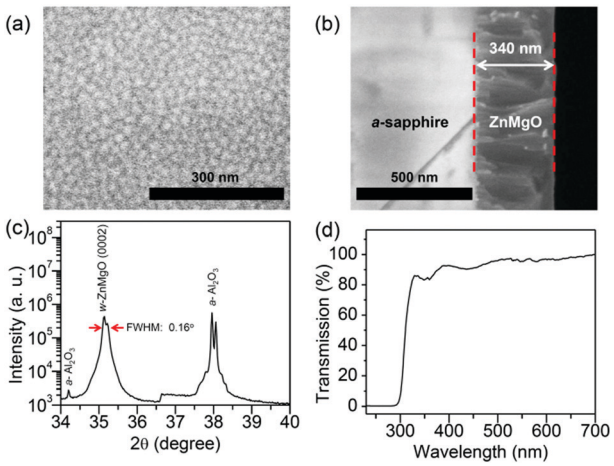

Fig. 2 (a) SEM images of ZnMgO films. (b) Cross sectional SEM images of ZnMgO films. (c) XRD patterns of ZnMgO films. (d) UV-Vis transmission spectra of ZnMgO films.

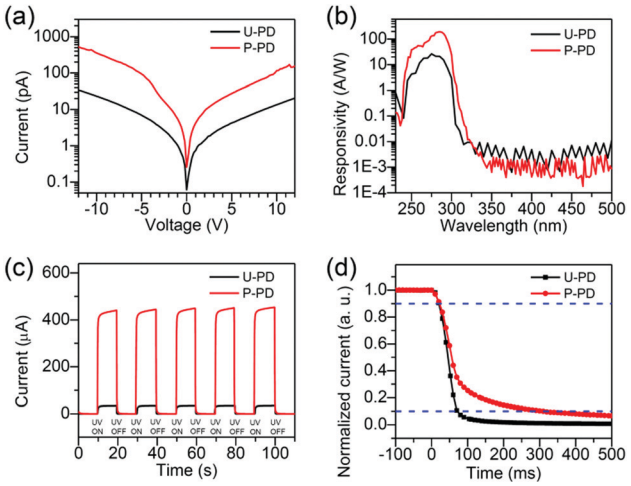

Fig. 3 (a) *I–V* characteristics of the unpackaged photodetector (U-PD) and packaged photodetector (P-PD) in dark. (b) Spectral responses of U-PD and P-PD under a bias of 10 V. (c) Time-dependent photocurrent response of U-PD and P-PD illuminated by 254 nm UV light with the intensity of 2 mW cm^{-2} under a bias of 10 V. (d) Decay edge of the current response under a bias of 10 V for U-PD and P-PD.

transmission spectrometry of the ZnMgO film. The transmittance of the sample in the visible range is more than 85%, and a very sharp optical transmission edge at ~4.1 eV (~300 nm) can be clearly observed.

An MSM photodetector was fabricated *via* photolithography and a wet etching procedure for the ZnMgO film. In this study, a direct wire bonding method between steel wires and photodetector by conductive silver adhesives is proposed. This simple and rapid direct bonding method does not require precise patterning and thickness of the metal contact areas *via* conventional wire bonding processes. In addition, a sealing treatment of the photodetector is proposed using silica gel, which can seclude the photodetector from atmosphere and humidity. The main advantages of using silica gel are as follows: the solar blind UV can penetrate the silica gel commendably (Fig. S2 in ESI†), thus the loss in responsivity of the packaged photodetector can be controlled in a relatively low level. The silica gel is inert and will not react with the ZnMgO material itself. Silica gel can effectively insulate the air, provide anoxic environment for the material surface, and improve the response of the device.

In order to investigate the effect of the sealing treatment on the photoresponse properties of the ZnMgO photodetector, the photoresponse performance of the unpackaged photodetector (U-PD) and packaged photodetector (P-PD) were measured.

The *I–V* characteristics in dark are shown in Fig. 3(a). After getting sealed by silica gel, the dark current increases from 13.6 pA to 115 pA under a bias of 10 V. Fig. 3(b) shows the responsivity of U-PD and P-PD under a bias of 10 V. It can be seen that the responsivity of the sample increases after the packaging. The maximum values of the two samples are 26 A W^{-1} and 191 A W^{-1}, respectively. The −3 dB cut-off wavelength is still maintained at about 295 nm, which is in good accordance with the optical transmission edge (Fig. 2(d)). The UV-visible rejection ratio, defined as the ratio between the peak responsivity and responsivity at 400 nm, can reach as large as 10^5 for P-PD. Fig. 3(c) shows the time-dependent response of the U-PD and P-PD. These results are measured by periodically turning on and off a 254 nm light under a bias of 10 V (turn on UV for 10 seconds, and turn off UV for 10 seconds, 254 nm light illumination with the intensity of 2 mW cm^{-2}). Upon the UV illumination, the current instantaneously increased to 34 μA and 440 μA for U-PD and P-PD, respectively. After turning off the light, the current quickly returned to their original values. The time-dependent response of the light on/off cycles shows good stability and reproducibility both for U-PD and P-PD. Fig. 3(d) shows the decay edges of the current of the U-PD and P-PD under a bias of 10 V. The decay time (defined as the time for the current dropping from 90% to 10% of the peak value) of U-PD and P-PD are 50 ms and 280 ms, respectively, indicating that a sealed environment has a disadvantageous effect on the recovery of dark current.

In order to investigate the effect of the sealed environment, the photocurrent of U-PD under a low pressure environment was measured (the pressure is around 1/30 standard atmospheric pressure, similar to a vacuum environment). The results are shown in Fig. 4. It can be seen that a longer carrier lifetime (response time) and a higher photocurrent are obtained in a low pressure

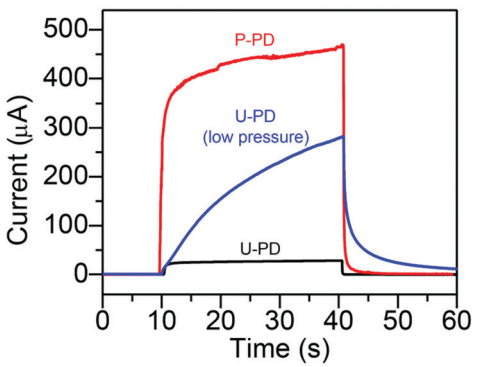

Fig. 4 The photocurrent of the packaged photodetector (P-PD) and unpackaged photodetector (U-PD) under different environments.

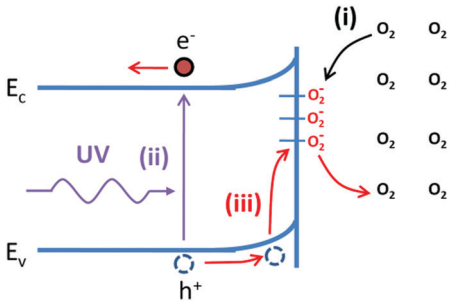

Fig. 5 Schematic oxygen-sensitized photoconduction mechanism of the ZnMgO films.

ambience in comparison to those in atmospheric pressure ambience. The photocurrent of the P-PD is the same as that of the U-PD under a relatively low pressure. It was reported that these phenomenon is caused by a so-called oxygen-sensitized photoconduction mechanism in metal oxide semiconductors, such as ZnO-based materials.

The photoconduction is a three-step process, which can be seen in Fig. 5: (i) in dark, oxygen molecules are adsorbed on the oxide surface and electron trapping sites are created. After free electrons are captured by the surface trapping state, the oxygen molecules turn into negative ions [$O_2(g) + e^- \rightarrow O_2^-(ad)$] that enhance the upward bending of the energy band at the surface. Furthermore, a low-conductivity depletion layer is formed near the surface. (ii) Under UV illumination, electron–hole pairs are created [$h\nu \rightarrow e^- + h^+$]. (iii) Holes migrate to the surface by following the built-in field imposed by the surface band bending and recombine with the negatively charged adsorbed oxygen ions [$h^+ + O_2^-(ad) \rightarrow O_2(g)$]. The excess holes are consumed mostly at the surface, resulting in a long lifetime of unpaired electrons, which dominate the photocurrent. Recombination took place while oxygen molecules could re-adsorb on the surface by the following steps: (i) according to this conventional model, the recombination rate of the excess electron is governed by the oxygen adsorption rate, which is expectedly much lower in oxygen-deficient ambience.

Fig. 6 shows schematics of the UV photoresponse process of U-PD, U-PD (under a low pressure), and P-PD. In dark, for U-PD, oxygen molecules are adsorbed on the surface of the ZnMgO film and capture the free electrons. As a result, a depletion layer with low conductivity is created near the surface of the film. When the U-PD works under a low pressure, the amounts of the adsorbed oxygen molecules become lower. Therefore, the adsorption–desorption

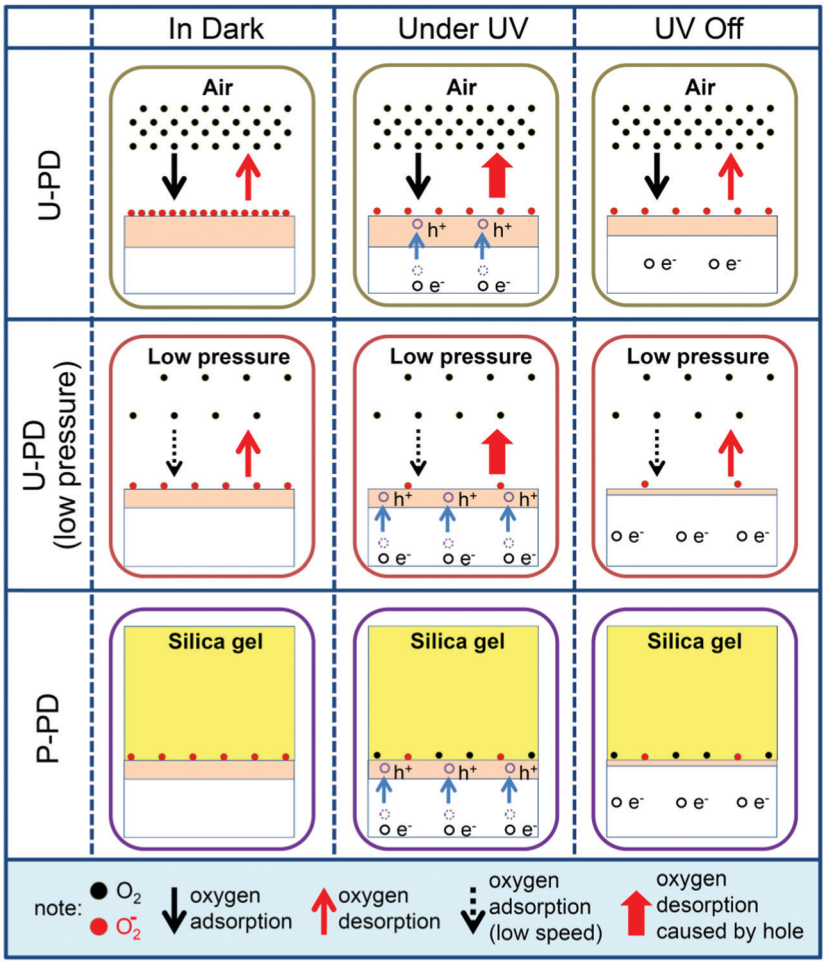

Fig. 6 Schematics of the UV photoresponse process of the unpackaged photodetector (U-PD), U-PD under low pressure, and packaged photodetector (P-PD).

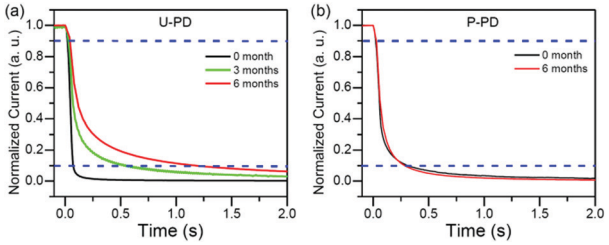

Fig. 7 Decay edges of the current response under a bias of 10 V for the (a) unpackaged photodetector (U-PD) and (b) packaged photodetector (P-PD) during different months.

equilibrium changes that reduces the thickness of the surface depletion layer, hence increasing the dark current. For P-PD, the silica gel insulates the air, creating conditions similar to those in a low pressure environment. Thus, the dark current of P-PD also increases.

When the devices are illuminated with UV light, for U-PD, the excess holes are consumed by reaction with oxygen negative ions, resulting in a long lifetime of unpaired electrons, which dominate the photocurrent. When the U-PD works under a low pressure, the amounts of the desorbed oxygen molecules increase due to the influence of an anoxic environment. Therefore, the excess holes are consumed increasingly and the responsivity increase. For P-PD, the desorbed oxygen retention on the interface of the ZnMgO film and silica gel only forms physical contact with the film. Although oxygen molecules are confined to the surface, photo-generated holes are indeed consumed more due to the influence of the anoxic environment, and thus the responsivity can still increase.

After turning off the UV light, the oxygen molecules are reabsorbed on the film. For P-PD, the path of oxygen adsorption maybe has a shorter distance than that in the low pressure environment; thus, the response speed of the device is faster than that in the low pressure environment. However, in the anoxic environment, the adsorption rate of oxygen is lower than that in the atmospheric pressure environment; hence, the response speed of P-PD is still slower than that of U-PD.

It is well known that the ZnMgO-based materials are very sensitive to the humidity and oxygen and the unpackaged ZnMgO-based photodetectors have a poor stability due to the influence of the humidity and oxygen. In order to investigate the influence of the humidity and oxygen on the photodetector, the decay edges of the current response under a bias of 10 V for U-PD and P-PD are measured during different months, and the results are shown in Fig. 7. It can be seen that as the U-PD is exposed to air for several months the 90–10% decay time gradually increases from 50 ms to 500 ms (3 months) and 1.17 s (6 months). On the contrary, the 90–10% decay time of P-PD maintains at around 280 ms. Because of the well-sealed packaged structure, the stability of the ZnMgO-based solar-blind photodetector obviously improved.

Table 1 shows the comparison between our device and typical high performance ZnMgO-based solar-blind photodetectors. It can be seen that few ZnMgO solar blind photodetectors could achieve both high responsivity, low dark current and fast response simultaneously. Moreover, there are no reports on the packaging of the ZnMgO-based UV photodetectors before our study. In our research, a packaged solar-blind photodetector are prepared, and it exhibited a relatively high responsivity and acceptable dark current and response speed. Moreover, the stability of the photodetector obviously improved due to the well-sealed packaged structure.

Conclusions

In this study, a packaged high performance ZnMgO solar-blind UV photodetector was prepared *via* a silica gel sealing treatment. A −3 dB cutoff wavelength of 295 nm and a responsivity of 191 A W^{-1} were achieved under a bias of 10 V. The 90–10% decay time of the device was 280 ms, and the dark current of the device was 115 pA under a bias of 10 V. Different from the traditional surface modification method, the silica gel cover was completely isolated from oxygen. The cover of silica gel provided an anoxic environment, which was similar to that when the unpackaged device was in a low pressure environment. In both cases, the responsivity of the device improved, but the decay time was shortened by the way of the silica gel coverage. The reason may be that when the device was exposed to UV light the desorption oxygen molecules were limited by silica gel and remained at the solid–solid interface between the silica gel and ZnMgO film. When the UV light was turned off, oxygen molecules were absorbed directly at the interface, which was easier. Therefore, the response speed of the device was faster than that of the unpacked device in the low pressure environment. Moreover, the stability of the ZnMgO-based solar-blind photodetector was obviously improved due to the well-sealed packaged structure. Our findings suggest that the sealing treatment of silica gel

Table 1 Comparison between our device and typical high performance ZnMgO-based solar-blind photodetectors

Sample	Responsivity (A W^{-1})	*I*-Dark (pA)	90–10% *t*-decay (ms)	Cutoff wavelength (nm)	Bias (V)	Package	Ref.
ZnMgO nanorods	2.01	560 000	—	270	5	No	39
ZnMgO films	1.664	0.25	∼1500	275	10	No	31
ZnMgO films	2	10	77	286	−5	No	13
ZnMgO films	48	35 000	0.45	273	10	No	12
ZnMgO films (U-PD 0 month)	26	13.6	50	295	10	No	This study
ZnMgO films (U-PD 6 month)	22	13.1	1170	295	10	No	This study
ZnMgO films (P-PD 0 month)	191	115	280	295	10	Yes	This study
ZnMgO films (P-PD 6 month)	205	111	280	295	10	Yes	This study

should be an effective method for the packaging of the unpackaged photodetector and improving the responsivity of the ZnMgO UV photodetector, which paves a new way for the fabrication of packaged solar-blind photodetectors.

Conflicts of interest

There are no conflicts to declare.

Acknowledgements

This work is supported by the National Natural Science Foundation of China under Grant (61605200, 61875194, 61475153, 11727902, 11704376, 61425021 and 61525404), Jilin Province Young and Middle-aged Science and Technology Innovation Leaders and Team Project (20180519023JH), Jilin Province Science Fund for Excellent Young Scholars (20180520173JH) and the 100 Talents Program of the Chinese Academy of Sciences.

Notes and references

1 Y. Xia, G. M. Zhai, Z. Zheng, L. Y. Lian, H. Liu, D. L. Zhang, J. B. Gao, T. Y. Zhai and J. B. Zhang, *J. Mater. Chem. C*, 2018, **6**, 11266.
2 S. Mitra, A. Aravindh, G. Das, Y. Pak, I. Ajia, K. Loganathan, E. Di Fabrizio and I. S. Roqan, *Nano Energy*, 2018, **48**, 551.
3 D. Y. Guo, H. Liu, P. G. Li, Z. P. Wu, S. L. Wang, C. Cui, C. R. Li and W. H. Tang, *ACS Appl. Mater. Interfaces*, 2017, **9**, 1619.
4 X. C. Guo, N. H. Hao, D. Y. Guo, Z. P. Wu, Y. H. An, X. L. Chu, L. H. Li, P. G. Li, M. Lei and W. H. Tang, *J. Alloys Compd.*, 2016, **660**, 136.
5 X. Zhou, Q. Zhang, L. Gan, X. Li, H. Q. Li, Y. Zhang, D. Golberg and T. Y. Zhai, *Adv. Funct. Mater.*, 2016, **26**, 704.
6 R. R. Zhuo, D. Wu, Y. G. Wang, E. P. Wu, C. Jia, Z. F. Shi, T. T. Xu, Y. T. Tian and X. J. Li, *J. Mater. Chem. C*, 2018, **6**, 10982–10986.
7 Y. R. Chen, Z. W. Zhang, H. Jiang, Z. M. Li, G. Q. Miao and H. Song, *J. Mater. Chem. C*, 2018, **6**, 4936.
8 S. Rathkanthiwar, A. Kalra, S. V. Solanke, N. Mohta, R. Muralidharan, S. Raghavan and D. N. Nath, *J. Appl. Phys.*, 2017, **121**, 164502.
9 F. Alema, B. Hertog, O. Ledyaev, D. Volovik, R. Miller, A. Osinsky, S. Bakhshi and W. V. Schoenfeld, *Sens. Actuators, A*, 2016, **249**, 263.
10 H. Y. Chen, P. P. Yu, Z. Z. Zhang, F. Teng, L. X. Zheng, K. Hu and X. S. Fang, *Small*, 2016, **12**, 5809.
11 M. M. Fan, K. W. Liu, X. Chen, Z. Z. Zhang, B. H. Li and D. Z. Shen, *RSC Adv.*, 2017, **7**, 13092.
12 H. Chen, X. Z. Ma, J. T. Zhang, Q. G. Li, H. Q. Liu, Z. X. Chen, G. Chu and S. Chu, *Opt. Mater. Express*, 2018, **8**, 785.
13 H. Chen, J. T. Zhang, Z. X. Chen, H. Q. Liu, X. Z. Ma, Q. G. Li, G. Chu and S. Chu, *J. Phys. D: Appl. Phys.*, 2018, **51**, 175104.
14 K. Arora, N. Goel and M. Kumar, *ACS Photonics*, 2018, **5**, 2391.
15 S. J. Cui, Z. X. Mei, Y. N. Hou, Q. S. Chen, H. L. Liang, Y. H. Zhang, W. X. Huo and X. L. Du, *Chin. Phys. B*, 2018, **27**, 067301.
16 W. Cui, Q. Ren, Y. S. Zhi, X. L. Zhao, Z. P. Wu, P. G. Li and W. H. Tang, *J. Nanosci. Nanotechnol.*, 2018, **18**, 3613.
17 T. He, Y. K. Zhao, X. D. Zhang, W. K. Lin, K. Fu, C. Sun, F. F. Shi, X. Y. Ding, G. H. Yu, K. Zhang, S. L. Lu, X. P. Zhang and B. S. Zhang, *Nanophotonics*, 2018, **7**, 1557.
18 Y. X. Liu, L. L. Du, G. D. Liang, W. X. Mu, Z. T. Jia, M. S. Xu, Q. Xin, X. T. Tao and A. M. Song, *IEEE Electron Device Lett.*, 2018, **39**, 1696.
19 S. Oh, C. K. Kim and J. Kim, *ACS Photonics*, 2018, **5**, 1123.
20 M. Pavesi, F. Fabbri, F. Boschi, G. Piacentini, A. Baraldi, M. Bosi, E. Gombia, A. Parisini and R. Fornari, *Mater. Chem. Phys.*, 2018, **205**, 502.
21 Y. K. Peng, Y. Zhang, Z. W. Chen, D. Y. Guo, X. Zhang, P. G. Li, Z. P. Wu and W. H. Tang, *IEEE Photonics Technol. Lett.*, 2018, **30**, 993.
22 H. Shen, Y. N. Yin, K. Tian, K. Baskaran, L. B. Duan, X. R. Zhao and A. Tiwari, *J. Alloys Compd.*, 2018, **766**, 601.
23 X. Wang, Z. W. Chen, D. Y. Guo, X. Zhang, Z. P. Wu, P. G. Li and W. H. Tang, *Opt. Mater. Express*, 2018, **8**, 2918.
24 Y. Xu, Z. Y. An, L. X. Zhang, Q. Feng, J. C. Zhang, C. F. Zhang and Y. Hao, *Opt. Mater. Express*, 2018, **8**, 2941.
25 D. Zhang, W. Zheng, R. C. Lin, T. T. Li, Z. J. Zhang and F. Huang, *J. Alloys Compd.*, 2018, **735**, 150.
26 Y. C. Chen, Y. J. Lu, C. N. Lin, Y. Z. Tian, C. J. Gao, L. Dong and C. X. Shan, *J. Mater. Chem. C*, 2018, **6**, 5727.
27 C. Yang, H. W. Liang, Z. Z. Zhang, X. C. Xia, P. C. Tao, Y. P. Chen, H. Q. Zhang, R. S. Shen, Y. M. Luo and G. T. Du, *RSC Adv.*, 2018, **8**, 6341.
28 X. Chen, K. W. Liu, Z. Z. Zhang, C. R. Wang, B. H. Li, H. F. Zhao, D. X. Zhao and D. Z. Shen, *ACS Appl. Mater. Interfaces*, 2016, **8**, 4185.
29 D. Y. Kim, J. H. Park, J. W. Lee, S. Hwang, S. J. Oh, J. Kim, C. Sone, E. F. Schubert and J. K. Kim, *Light: Sci. Appl.*, 2015, **4**, e263.
30 T. Takagi, H. Tanaka and S. Fujita, *Jpn. J. Appl. Phys., Part 2*, 2003, **42**, L401.
31 M. M. Fan, K. W. Liu, Z. Z. Zhang, B. H. Li, X. Chen, D. X. Zhao, C. X. Shan and D. Z. Shen, *Appl. Phys. Lett.*, 2014, **105**, 011117.
32 X. Chen, K. Liu, X. Wang, B. Li, Z. Zhang, X. Xie and D. Shen, *J. Mater. Chem. C*, 2017, **5**, 10645.
33 M.-M. Fan, K.-W. Liu, X. Chen, X. Wang, Z.-Z. Zhang, B.-H. Li and D.-Z. Shen, *ACS Appl. Mater. Interfaces*, 2015, **7**, 20600.
34 C. H. Tian, D. Y. Jiang, Z. D. Tan, Q. Duan, R. S. Liu, L. Sun, J. M. Qin, J. H. Hou, S. Gao, Q. C. Liang and J. X. Zhao, *Mater. Res. Bull.*, 2014, **60**, 46.
35 D. Y. Jiang, C. G. Tian, G. Yang, J. M. Qin, Q. C. Liang, J. X. Zhao, J. H. Hou and S. Gao, *Mater. Res. Bull.*, 2015, **67**, 158.
36 C. T. Lee, T. S. Lin and C. H. Chen, *J. Electron. Mater.*, 2015, **44**, 4722.
37 P. Murkute, H. Ghadi, S. Patil, H. Rawool, S. Pandey and S. Chakrabarti, *Sens. Actuators, B*, 2018, **256**, 204.
38 F. Ahmed, N. Arshi, M. S. Anwar, R. Danish and B. H. Koo, *Curr. Appl. Phys.*, 2013, **13**, S64.
39 C. Z. Wu, L. W. Ji, S. M. Peng, Y. L. Chen and S. J. Young, *Electrochem. Solid-State Lett.*, 2011, **14**, J55.

